DOI: 10.1002/((please add manuscript number))

Article type: Communication

Lead-Free Inverted Planar Formamidinium Tin Triiodide Perovskite Solar Cells Achieving Power Conversion Efficiencies up to 6.22%

Weiqiang Liao,[†] Dewei Zhao,[†,] Yue Yu, Corey R. Grice, Changlei Wang, Alexander J. Cimaroli, Philip Schulz, Weiwei Meng, Kai Zhu, Ren-Gen Xiong,*and Yanfa Yan**

Weiqiang Liao,[†] Dr. Dewei Zhao,[†] Yue Yu, Corey R. Grice, Changlei Wang, Alexander J. Cimaroli, WeiweiMeng, and Prof. Yanfa Yan

Department of Physics and Astronomy and Wright Center for Photovoltaics Innovation and Commercialization, The University of Toledo, Toledo, OH 43606, United States

* Corresponding authors' emails:

D.Z.: dewei.zhao@utoledo.edu

Y.Y.: yanfa.yan@utoledo.edu

Weiqiang Liao and Prof. Ren-Gen Xiong

Ordered Matter Science Research Center, Southeast University, Nanjing 211189, P. R. China.

* Corresponding authors' email:

R.G.X.: xiongrg@seu.edu.cn

Dr. Philip Schulz and Dr. Kai Zhu

Chemistry and Nanoscience Center, National Renewable Energy Laboratory, Golden, Colorado 80401, United States

[†]These authors contributed equally to this work.

Keywords:
Pb-free perovskite solar cells, $FASnI_3$, pinhole-free, uniform perovskite, SnF_2 additives

Organic-inorganic lead (Pb) halide perovskite solar cells (PVSCs) are considered as a promising photovoltaic technology for low-cost solar energy conversion due to the remarkable progress on the power conversion efficiencies (PCEs) made in the past few years, boosting from 3.8% to 22.1%.[1-19] However, the use of toxic Pb severely limits their broad applications and commercialization. The development of Pb-free PVSCs is highly desirable and has drawn significant attention. Theoretical studies have shown that the superior photovoltaic properties of Pb halide perovskites are partly attributed to the perovskite structure and the inactive Pb6s orbitals.[20-23] It has been suggested that Pb^{2+} can be replaced with other cations that are environmentally friendly and also contain inactive outer shell s orbitals such as germanium (II) (Ge^{2+}),[24] tin (II) (Sn^{2+}),[25, 26] antomony (III) (Sb^{3+}),[27] and bismuth (III) (Bi^{3+})[28] to form Pb-free PVSCs.[29, 30] Among these cations, only Sn^{2+}-based PVSCs have achieved reasonable device performance. So far, Snaith's and Kanatzidis's groups have independently demonstrated methylammoniumtin iodide ($MASnI_3$) based Pb-free PVSCs with PCEs of around 6%in 2014.[25, 26] These reports have stimulated considerable follow-up studies on Pb-free Sn-based PVSCs.[31-37] However, since 2014, no further improvement of the PCEs of Pb-free Sn-based PVSCs was reported, while the PCEs of Pb halide PVSCs have been significantly advanced within the past few years.

The lack of progress on improving performance of Pb-free Sn-based PVSCs may be due to several challenging factors: (1) $MASnI_3$ PVSCs are not stable due to the facile oxidization of Sn^{2+} to Sn^{4+}. $MASnI_3$ PVSCs typically degrade rapidly in air, leading to higher carrier density and conductivity and thus significant electrical shorting of the devices.[31] This makes the likelihood of reproducibly fabricating $MASnI_3$ PVSCs extremely low. (2) It is difficult to

synthesize uniform and fully covered Sn-based thin films without additives due to the rapid crystallization of Sn-based perovskite at room temperature.[36] (3) Most Pb-free Sn-based PVSCs use the regular cell structure, in which hole selective layers (HSLs) are deposited on the Sn-based perovskite layers. High-performance HSLs, such as 2,2′,7,7′-Tetrakis (N,N-di-p-methoxyphenylamino)-9,9′-spirobifluorene (Spiro-OMeTAD) and poly(triarylamine) (PTAA) typically contain lithium (Li) and orcobalt (Co) salts that damage the Sn-based perovskite films and lead to poor device performance.[25, 26, 32, 34, 36] To further advance the performance of Pb-free Sn-based perovskite devices, these challenging issues must be resolved with some progress having already been made. For example, Kanatzidis's group and Mathews's group have reported that tin fluoride (SnF_2) additives can effectively suppress the oxidization of Sn^{2+} and reduce the hole density in the resulting films.[31, 38] It has been also reported that formamidinium tin triiodide ($FASnI_3$) is more stable than $MASnI_3$.[37] Formation of a transitional SnI_2·3 dimethyl sulfoxide (DMSO) intermediate phase and the addition of SnF_2 are effective approaches to obtain highly uniform and pinhole-free Sn-based perovskite films.[31, 32]Very recently, Seok's group has shown that fully covered $FASnI_3$ films can be obtained by using solvent engineering and SnF_2-pyrazine complex as additives.[33] However, the highest efficiency of 4.8% is still much lower than the best PCE reported for $MASnI_3$ PVSCs two years ago. Meanwhile, the use of mesoporous TiO_2 as electron selective layers (ESLs) in regular device architecture devices requires high temperature sintering, which is not preferred for large-scale manufacturing.

Here, we report on the first reproduction of efficient Pb-free Sn-based PVSCs with PCEs of up to 6.22% after the reports by Snaith's and Kanatzidis's groups in 2014. Aside from the

common practices in fabrication of Pb-free Sn PVSCs such as using a $FASnI_3$ absorber, SnF_2 additives in the precursors, and solvent engineering, we used two additional strategies to overcome the above described challenging issues for fabricating efficient Pb-free Sn-based PVSCs. Firstly, we used a simple inverted device architecture to avoid the use of salt-doped HSLs which damage the $FASnI_3$ perovskites and to reduce current density-voltage (*J-V*) hysteresis. Our $FASnI_3$ PVSCs have the cell architecture of indium tin oxide (ITO)/poly(3,4-ethylenedioxythiophene):polystyrene sulfonate (PEDOT:PSS)/$FASnI_3$/fullerene (C_{60})/2,9-dimethyl-4,7-diphenyl-1,10-phenanthroline (BCP)/Ag. Secondly, we used SnF_2 additives and diethyl ether dripping in solvent engineering process to synthesize high-quality, uniform, and fully covered $FASnI_3$ perovskite thin films. With 10 mol% SnF_2 additives, we were able to produce densely and fully covered $FASnI_3$ perovskite films with a hole density of approximately $10^{17}/cm^3$ and an optical band gap of approximately 1.40 eV. The high-quality $FASnI_3$ films allowed us to fabricate efficient Pb-free Sn-based PVSCs with high reproducibility. For 30 cells with an active area of 0.04 cm^2 fabricated in this fashion, we have achieved an average PCE of 5.41±0.46% with an average open-circuit voltage (V_{oc}) of 0.449±0.023 V, an average short-circuit current density (J_{sc}) of 20.69±0.95 mA/cm^2, and an average fill factor (FF) of 58.20±2.50% under forward voltage scan. The champion cell has obtained a PCE of 6.22 (6.07%) measured under forward (reverse) voltage scan and a steady-state efficiency of ~6.00% for 100s. Our encapsulated cells have good long-term illumination stability. For example, a cell with an initial efficiency of 5.80% only showed a decrease in PCE by 5.50% over a period of 2700 s. We have also fabricated 30 cells with an active area of 0.12 cm^2, which exhibited similar device performance. The light-intensity dependence

characterization reveals that the V_{oc}s of these cells are limited by the imbalanced charge transport at the PEDOT:PSS/$FASnI_3$ and $FASnI_3$/C_{60} interfaces. Higher PCEs are anticipated if these interface problems can be resolved. Our results confirm that efficient Pb-free Sn-based PVSCs can be fabricated and suggest that the inverted planar device architecture and diethyl ether dripping are promising approaches to further enhance the performance of Pb-free Sn-based PVSCs.

We used the one-step solution process combined with solvent engineering process to produce dense and uniform $FASnI_3$ perovskite thin films.[31-33] As reported in literature, the solvent engineering approach involves the use of mixed N,N-dimethylmethanamide (DMF) and DMSO solvents and the antisolvent dripping.[39] The presence of DMSO is critical for forming high-quality Sn-based perovskite films as it forms the important SnI_2·3DMSO intermediate phase.[32] Antisolvent dripping is another critical process to produce high-quality perovskite films.[33] So far, chlorobenzene and toluene are popular choices for the antisolvent dripping. However, we found that these antisolvent dripping agents do not form densely and fully conformal $FASnI_3$ perovskite thin films on PEDOT:PSS coated ITO/glass substrates. **Figure S1** shows the scanning electron microscopy (SEM) images of $FASnI_3$ films deposited on PEDOT:PSS by different antisolvent drippings. The processing without antisolvent dripping led to a discontinuous $FASnI_3$ film with large grains (**Figure S1a**). Dripping with chlorobenzene (**Figure S1b)** improved the surface coverage of the $FASnI_3$ films; however the films exhibited hierarchical morphology with rougher surface and pinholes. Dripping with toluene further improved the coverage of $FASnI_3$ perovskite films (**Figure S1c**), but pinholes still exist and surface is rough due to island formation, which is different from the case of

$FASnI_3$ deposition on mesoporous TiO_2.[33] Dripping with diethyl ether produced the best $FASnI_3$ thin films on PEDOT:PSS (**Figure S1d**). The surface morphology of this $FASnI_3$ film is highly uniform and completely covers the substrate. This dripping process has also been used to produce high-quality Pb-based perovskite thin films in our previous study[40] and Park's study.[41] We found that $FASnI_3$ perovskites form very rapidly with either chlorobenzene or toluene dripping. The spin-coated films turned black immediately when chlorobenzene or toluene was dripped onto the films. The color of the films did not change much after post-deposition annealing at 70 ^{o}C. However, dripping by diethyl ether led to a formation of reddish film. The color changed to black after a time period of around 40s. Therefore, using diethyl ether dripping in solvent engineering process is an important step towards our successful fabrication of efficient Pb-free $FASnI_3$ PVSCs with the inverted planar cell architecture.

The amount of SnF_2 in the $FASnI_3$ precursor is also crucial for optimizing the film morphology and controlling the charge carrier density and conductivity of the resulting $FASnI_3$ thin films.[31] We found that the surface coverage of the $FASnI_3$ film on PEDOT:PSS is remarkably dependent on the amount of SnF_2. Flower-like structures and many pinholes are observed on the surface of pure $FASnI_3$ films grown on PEDOT:PSS (**Figure 1a**). When 5 mol% SnF_2 additives are added into the $FASnI_3$ precursor, the flower-like structures disappear and the $FASnI_3$ films become more uniform in appearance. However, pinholes formation within the film still occurs (**Figure 1b**), albeit at a lower density than observed for the samples without SnF_2. When the SnF_2 concentration is increased to 10 mol%, 15 mol%, and 20 mol% (**Figure 1c-e**), highly uniform and compact $FASnI_3$ films are obtained without

any pinholes. However, for 15 mol%SnF_2 additives, rod-like bright regions on the surface of $FASnI_3$ films start to appear (**Figure 1d**). It becomes prominent for the films with 20 mol% SnF_2 additives (**Figure 1e**). In order to elucidate the origin and nature of these rod-like bright regions, SEM-energy-dispersive X-ray spectroscopy (SEM-EDS) has been performed on these bright regions. The emission peak of elemental fluoride is found present, indicating they are SnF_2 residues (**Figure S2**). 30 mol% SnF_2 produces discontinuous $FASnI_3$ films with more rod-like bright regions at the aggregated grain boundaries (**Figure 1f**).

The $FASnI_3$ perovskite films produced by solvent engineering with diethyl ether dripping exhibit very strong crystallinity. An X-ray diffraction (XRD) pattern obtained from a $FASnI_3$ perovskite film with 10 mol% SnF_2 additives is shown in **Figure 2a**, confirming that the perovskite film is crystalline with the orthorhombic structure and random orientation, which is consistent with our calculated patterns and the previously reported.[33, 37] We found that the molar concentration of SnF_2 additives does not significantly change the crystallinity of the $FASnI_3$ films: the $FASnI_3$ perovskite films with different concentration of SnF_2 additives have almost identical XRD patterns as shown in **Figure S3**. **Figure 2b** shows the absorption spectrum of the $FASnI_3$ perovskite film with 10 mol% SnF_2 additives, exhibiting an absorption onset of 900 nm, in good agreement with that reported by other groups.[33]As mentioned above, the addition of SnF_2 reduces the carrier density and conductivity in the $FASnI_3$ film. The charge carrier densities of the $FASnI_3$ film with varying SnF_2 concentration were extracted from capacitance–voltage (C-V) measurements. The dependence of carrier densities on SnF_2 molar concentration is plotted in **Figure 2c**. $FASnI_3$ films without SnF_2 have a relatively high carrier density of $3.12\pm1.08\times10^{19}/cm^3$, however, with the addition of

SnF_2, the charge carrier density is decreased by roughly two orders of magnitude to a range of $1\sim2\times10^{17}/cm^3$ ($1.73\pm0.13\times10^{17}/cm^3$, $1.31\pm0.17\times10^{17}/cm^3$, $1.07\pm0.05\times10^{17}/cm^3$, and $1.13\pm0.04\times10^{17}/cm^3$ for 5 mol%, 10 mol%, 15 mol%, and 20 mol% SnF_2, respectively), which is more suitable for solar cell applications. The carrier density does not appear to be very strongly dependent on the SnF_2 concentration, but merely the presence of SnF_2. However, if the concentration of SnF_2 is more than 10mol%, SnF_2 secondary phase starts to appear, which may not be beneficial for solar cell performance. We also performed time-resolved photoluminescence (TRPL) measurement to extract charge carrier lifetime in $FASnI_3$ films with 10 mol% SnF_2 additives. As shown in **Figure 2d**, the carrier lifetime is 6.8 ns, which is much shorter than that in $MAPbI_3$ based perovskite.[40] Nonetheless, the $FASnI_3$ perovskite films with 10 mol% SnF_2 additives led to inverted planar PVSCs with the best PCEs in this study.

Figure 3a shows a cross-sectional SEM image of our inverted planar $FASnI_3$ PVSCs with a structure of ITO/PEDOT:PSS/$FASnI_3$/C_{60}/BCP/Ag. The PEDOT:PSS and C_{60} serve as the HSLs and ESLs, respectively. The $FASnI_3$ perovskite film appears to be compact and free of voids and pinholes. **Figure 3b** shows a possible energy band diagram of our $FASnI_3$ PVSCs. The lowest unoccupied molecular orbital (LUMO) level and the highest occupied molecular orbital (HOMO) level of C_{60} are taken from the literature.[11, 42-46] The energy position of the valence band maximum (VBM) of $FASnI_3$ is taken from the report.[37] It seems that the LUMO level of C_{60} is matched with the conduction band minimum (CBM) of $FASnI_3$, facilitating effective electron transfer from $FASnI_3$ to Ag cathode. Meanwhile, the HOMO of C_{60} is lower than the VBM of $FASnI_3$, blocking the holes from $FASnI_3$. Thus, C_{60}

suppresses charge recombination at the interface and shunt currents.[47] A thin layer of BCP enhances the contact between the C_{60} and the Ag electrode.[45, 48, 49] PEDOT:PSS works as an anode buffer layer and HSL to transport holes from $FASnI_3$ to ITO anode. It should be noted that report on the VBM level of $FASnI_3$ is scarce in literature.[37, 50] The reported VBM levels of $MASnI_3$ in literature vary largely.[50-52] It is likely that the easy oxidation of Sn^{2+} to Sn^{4+} on the surface of Sn-based perovekiste thin films makes the reliable measurement of the VBM level using ultra-violet photoelectron spectroscopy (UPS) difficult due to the sensitivity of UPS technique to the film surface. Therefore, the energy levels shown in **Figure 3b** may change when more reports on experimental measurement become available. Nonetheless, the energy diagram shown in **Figure 3b** is not ideal for optimal device performance: the HOMO level of PEDOTS:PSS is slightly high in energy, while the HOMO level of C_{60} is not low enough. Additional work on HSL and ESL optimization and interface engineering are needed to further enhance the performance of Pb-free Sn-based PVSCs.

The use of C_{60} as the ESL allows us to deposit the ESL layer onto $FASnI_3$ perovskite thin films by thermal evaporation. The cross-sectional SEM image (**Figure 3a**) of a finished device clearly displays the layers stacked in our $FASnI_3$ cell. The grain size of the perovskite along the normal of the perovskite film on PEDOT:PSS is apparently larger than the thickness (around 500 nm) of the perovskite film, which leads to the absence of grain boundaries along the direction of carrier transport in the device and thus largely mitigates charge recombination at the grain boundaries.[43] Therefore, the large grains (inset of **Figure 1c**) are expected facilitate more efficient charge extraction. A combined thin bilayer of C_{60} and BCP, as well as the top Ag electrode, are thermally deposited onto the perovskite layer,

following the topology of the perovskite layer. It is necessary to emphasize the advantages of vacuum evaporation technique in our work since the materials (C_{60}, BCP and Ag) can be uniformly and evenly deposited on the $FASnI_3$ perovskite layer, i.e. complete coverage of perovskite surface by C_{60} and BCP. Therefore, this vacuum deposition approach significantly prevents the formation of shunting pathways, resulting in efficient PVSCs with good FFs.[45]

Our champion $FASnI_3$ PVSC with an active area of 0.04 cm^2 and with 10 mol% SnF_2 achieves a maximum PCE of 6.22 (6.07)% with a V_{oc} of 0.465 (0.456) V, a J_{sc} of 22.07 (22.07) mA/cm^2, and an FF of 60.67 (60.23)% under forward (reverse) voltage scan, exhibiting very small *J-V* hysteresis behavior, which is attributed to the inverted device architecture and fullerene usage.[53] Its *J-V* characteristics under 100 mW/cm^2 AM1.5G illumination and external quantum efficiency (EQE) spectrum are shown in **Figure 4a and b**. The EQE-integrated J_{sc} can reach 22.03 mA/cm^2, in good agreement with that obtained from the *J-V* curve. To verify the device performance, the steady-state efficiency measurement has been performed to reflect the actual performance under operation. Its steady-state photocurrent at a constant bias of 0.344 V for 100 s under 100 mW/cm^2 AM1.5G illumination is approximately 17.45 mA/cm^2, corresponding to a stabilized output power of ~6.00%, as shown in **Figure 4c**. The steady-state efficiency is close to the PCE from *J-V* curves. To the best of our knowledge, this is the highest steady-state efficiency reported for Pb-free Sn-based PVSCs to date. In order to verify the reproducibility of our devices using 10% SnF_2 additives, we fabricated 30 devices in several batches. As shown in the histogram of the corresponding device data in **Figure 4d**, the average PCE is 5.41±0.46% with average V_{oc} of 0.449±0.023 V, average J_{sc} of 20.69±0.95 mA/cm^2, and average FF of 58.20±2.50% under forward voltage scan. We have also fabricated $FASnI_3$ PVSCs with a larger active area of 0.12 cm^2 and 10 mol% SnF_2 additives. The *J-V* curves of the best-performing device and the PCE histogram of 30 cells shown in **Figure S4**. These cells

achieved comparable performance with the cells with smaller active areas, yielding the average PCE of 5.38±0.32% with average V_{oc} of 0.466±0.019 V, average J_{sc} of 20.58±0.61 mA/cm^2, and average FF of 56.13±1.39% under forward voltage scan, among which the best-performing cell showed a PCE of 6.03 (5.99)% with a V_{oc} of 0.481 (0.484) V, a J_{sc} of 21.92 (21.83) mA/cm^2, and an FF of 57.23 (56.10)% measured under forward (reverse) voltage scan. Therefore, our devices with 10% SnF_2 additives appear to be highly reproducible.

It has been reported that the improvement of $FASnI_3$ perovskite morphology by addition of SnF_2or pyrazine leads to an increase in the corresponding device performance in regular structure, in which SnF_2 additives are crucial to inhibit the formation of Sn^{4+} in $FASnI_3$ perovskite and to produce pinhole-free $FASnI_3$ perovskite films.[33, 37] In order to examine the effect of SnF_2 concentration on the cell performance and relationship between film morphology and device performance, the $FASnI_3$ PVSCs with various molar concentration of SnF_2 have been fabricated. Their photovoltage parameters are summarized in **Figure S5** and **Table S1**. Without SnF_2 additives, the $FASnI_3$ cells show rather low efficiencies of 0.57±0.09%. When SnF_2 is added into the $FASnI_3$, all parameters are improved largely. It is obvious that the average J_{sc}s, V_{oc}s, and FFs increase firstly and then decrease with the increase of SnF_2 concentration, in which the J_{sc} has relatively small change. The trend of cell performance is consistent with the observed trend in film morphology in which the pinholes in $FASnI_3$ films are firstly reduced and then disappear with the increase of SnF_2 additives. However, secondary phase starts to form when the SnF_2 concentration is more than 10 mol% and the film starts to become discontinuous when the SnF_2 molar concentration is increased to 30 mol%.

The $FASnI_3$ PVSCs with 10 and 15 mol% SnF_2 achieve close average V_{oc}s (0.460±0.015 V and 0.430±0.005 V) and FFs (58.88±1.68% and 57.21±0.89%), respectively, since both of them have similar surface coverage, leading to average PCEs of 5.59±0.23% and 4.62±0.13%, respectively. The only difference is that the film with 15 mol% SnF_2 additives has some rod-like bright regions on the surface, which have been confirmed as SnF_2 in abovementioned SEM-EDS results. With the increase of SnF_2 to 20 mol%, residual SnF_2 grains become greater in number and are mostly located at the grain boundaries, resulting in reduced average PCEs of 4.06±0.13%. Furthermore, with 30 mol% SnF_2 additives, the $FASnI_3$ aggregated into large group of grains and some SnF_2 additives exist on top of $FASnI_3$perovskite surface. However, due to the stress during film coating, obvious pinholes appear to be present again, leading to significant reduction in V_{oc} and FF. The observed trend for the dependence of device performance on the amount of SnF_2 is similar to previously reported work on SnF_2:pyrazine complex as additives in $FASnI_3$ PVSCs.[33] In other words, the morphology of the $FASnI_3$ is a critical factor in high-efficiency Sn-based PVSCs. It is worth mentioning that the relatively high performance of the devices with SnF_2 additives in our work might be attributed to (1) ultra-compact and uniform $FASnI_3$ perovskite film, leading to relatively reduced charge recombination; (2) use of inverted device architecture, in which C_{60} passivates the perovskite surface and transports electrons.[53] Moreover, our $FASnI_3$ PVSCs with 10 mol% SnF_2 additives exhibit very little dependence of device performance on the scanning speed as shown in **Table S2**.

It is also worth highlighting that our encapsulated cell showed a good long-term illumination stability under continuous 100 mW/cm^2 AM1.5G illumination as shown in

Figure 5a. It showed a 5.50% drop in efficiency (photocurrent density) over a period of 2700 s, from its initial efficiency of 5.80% (16.68 mA/cm^2) to 5.48% (15.70 mA/cm^2). The encapsulated cells stored in dark and glove box exhibited a good stability for 30 days (**Figure 5b**), maintaining 85% of its initial efficiency of ~5.60% when measured in ambient. The degradation of our encapsulated cells is likely due to the use of organic materials as charge transport layers and the measurement under ambient condition. A recent report from Seok's group also presents that the encapsulated $FASnI_3$ PVSCs can be stable for over 100 days.[33] All these encouraging results suggest that Pb-free $FASnI_3$PVSCs can be made stable through encapsulation.

The PCEs of our $FASnI_3$ PVSCs are mainly limited by the V_{oc}s. Snaith's group has reported a V_{oc} of 0.88 V for their best $MASnI_3$ PVSCs.[26] If a similar V_{oc} were obtained in our $FASnI_3$ PVSCs, PCEs over 10% should be expected. To understand the limiting mechanism of the V_{oc} of our $FASnI_3$ PVSCs, we measured the *J-V* characteristics of the device with 10 mol% SnF_2 additives under different light intensities ranging from 1 to 100 mW/cm^2. **Figure 6a** shows the power law dependence of J_{sc} on light intensity ($J \propto I^{\alpha}$), which exhibits a linear relation on a double logarithmic scale with $\alpha = 0.85$. A solar cell with no space charge effect will have an α value close to 1 and the one with space charge effect will have an α value equal to 0.75.[54-56] Therefore, our devices with 10 mol% SnF_2 additives appear to be space charge limited. This could be ascribed to the charge carrier imbalance resulting from the interfacial barriers at the interface between charge transport layers and $FASnI_3$ perovskite layer.[43, 45, 54-57] **Figure 6b** shows V_{oc} as a function of logarithmic light intensity. V_{oc} increases monotonically with logarithmic light intensity. A trap-free relationship should have a slope of $\delta V_{oc} = kT/q$.[58, 59] Here, the slope of $\delta V_{oc} = 1.21kT/q$ implies trap-assisted Shockley-Read-Hall recombination prevalent in our $FASnI_3$ PVSCs with 10 mol% SnF_2 additives.[60-62] Therefore, the V_{oc}'s of our $FASnI_3$ PVSCs are

limited by charge recombination at $FASnI_3$/PEDOT:PSS or $FASnI_3/C_{60}$ interface or in the $FASnI_3$ absorbers. The interface recombination can be reduced through interface engineering or using alternative HSL and/or ESL materials. The recombination in $FASnI_3$ absorbers can be further reduced by carefully controlling the amount of SnF_2 concentration and synthesis process of the $FASnI_3$ thin films. Therefore, there is still large room to improve the performance of Sn-based PVSCs.

In summary, we have demonstrated efficient Pb-free planar $FASnI_3$PVSCs with a simple inverted device architecture, consisting of PEDOT:PSS HSLs and C_{60} ESLs. We found that antisolvent dripping using diethyl ether together with the use of SnF_2 additives is critical for synthesizing highly uniform and pinhole-free compact $FASnI_3$ perovskite thin films with charge carrier density values suitable for solar cell applications. Our Pb-free $FASnI_3$ PVSCs with 10 mol% SnF_2 additives have achieved average PCEs of 5.41±0.46% and maximum PCE of 6.22% under forward voltage scan, exhibiting small *J-V* hysteresis. The champion cell shows a steady-state efficiency of ~6.0% for over 100s. The encapsulated cells have shown good long-term illumination stability with a 5.50% decrease of its initial efficiency of 5.80% over a period of 2700 s. The use of diethyl ether dripping in solvent engineering process and the inverted cell architecture are critical for fabricating efficient Pb-free $FASnI_3$ PVSCs with high reproducibility. Our results confirm that it is practical to fabricate efficient Pb-free Sn-based PVSCs and provide important progress in realizing stable and highly efficient environmentally friendly PVSCs.

Experimental Section

Film preparation:

The $FASnI_3$ precursor solution without SnF_2 was prepared by dissolving 372 mg of SnI_2 (Sigma-Aldrich) and 172 mg of formamidinium iodide (FAI) (Dyesol) in 800 µL N,N-dimethylmethanamide (DMF) (anhydrous, Sigma-Aldrich) and 200 µL dimethyl sulfoxide (DMSO) (anhydrous, Sigma-Aldrich). For precursor solution with SnF_2 addition, 5, 10, 15, 20, and 30 mol % of SnF_2 (Sigma-Aldrich, 99%) was added to the above perovskite solution, respectively. The samples for SEM measurement were obtained by spin-coating these precursor solutions without and with SnF_2additives onto ITO/PEDOT:PSS. Chlorobenzene, toluene, and diethyl ether was dripped onto the spinning substrate during the spin-coating. All perovskite films were made and annealed at 70°C for 20 min in a glovebox. The samples used for TRPL measurements were coated by a 30 nm thick film of poly(methyl methacrylate) (PMMA).

Device fabrication:

The pre-patterned ITO substrates were cleaned by ultra-sonication in diluted Micro-90 detergent, deionized water, acetone, and isopropanol for 15 min, respectively. PEDOT:PSS films were coated on the cleaned ITO substrate at 4000 rpm for 50 s and then dried at 175 °C for 30 min.$FASnI_3$ films were deposited by spin-coating the precursor solution with and without SnF_2 additives onto PEDOT:PSS film at 4000 rpm for 60s in a glove box. Diethyl ether was dripped onto the spinning substrate during the spin-coating as discussed. The perovskite films were then annealed at 70 °C for 20 min. Finally, C_{60} (20 nm)/BCP (5 nm)/Ag (75 nm) were sequentially deposited by thermal evaporation to complete

the fabrication. The active areas of the devices were 0.04 cm^2 and 0.12 cm^2. Devices were encapsulated with cover glass and UV-curable epoxy.

Film and device characterization:

Perovskite films were imaged with a high resolution field emission scanning electron microscope (SEM)(Hitachi S-4800). The crystal structure of the $FASnI_3$ films with various SnF_2 concentrations was examined by X-ray diffraction (XRD) (Rigaku Ultima III) with Cu Kα radiation under operation conditions of 40 kV and 44 mA. Simulated XRD pattern based on refined structure from literature[63, 64] was generated with Mercury Software (Cambridge Crystallographic Data Centre).[65] The absorption spectra of the $FASnI_3$ perovskite film on PEDOT:PSS were measured by UV-Vis spectrophotometer (PerkinElmer Lambda 1050). All layer thicknesses were determined using a Dektak surface profiler and calibrated by ellipsometer. Capacitance-voltage (C-V) measurements were conducted using a Solartron Modulab potentiostat (Ametek Inc.) equipped with a 1MHz frequency response analyzer module. A perturbation voltage of 10mV at a frequency of 20 kHz was superimposed upon the DC potential bias to yield the resulting C-V curves, which was scanned in both the forward and reverse bias directions at a rate of 20 mV/s. The measurements were performed at room temperature under dark conditions, with the exclusion of ambient light. Average carrier concentrations for the perovskite layers were extracted from this data using a Mott-Schottky analysis.[66] TRPL was measured with a Hamamatsu streak camera system (C10910-05), while the excitation source is a Fianium Supercontinuum high power broadband fiber filter (SC400-2-PP). The chosen excitation wavelength was 530 nm at ~ 25 µW power on a spot size of 0.02 mm^2. The decay curve of PL emission was fitted using a single exponential model. *J-V* curves were measured in air under 100 mW/cm^2 AM1.5G solar irradiation (PV Measurements Inc.) with a Keithley 2400 Source

Meter. EQE spectra were performed on a QE system (PV Measurements Inc.). Light intensity measurements were made by decreasing the solar irradiation with neutral density light filters. All characterizations and measurements were performed in the ambient.

Supporting Information

Supporting Information is available from the Wiley Online Library or from the author.

Acknowledgements

This work is financially supported by the U.S. Department of Energy (DOE) SunShot Initiative under the Next Generation Photovoltaics 3 program (DE-FOA-0000990), National Science Foundation under contract no. CHE−1230246 and DMR−1534686, and the Ohio Research Scholar Program. The work at the National Renewable Energy Laboratory issupported by the U.S. Department of Energy SunShot Initiative under the Next Generation Photovoltaics 3 program (DE-FOA-0000990) under Contract No. DE-AC36-08-GO28308. This research used the resources of the Ohio Supercomputer Center and the National Energy Research Scientific Computing Center, which is supported by the Office of Science of the U.S. Department of Energy under Contract No. DE-AC02-05CH11231. The work at Southeast University (P.R. China) is supported by National Natural Science Foundation of China (NSFC) under Contract No. 91422301.

Received: ((will be filled in by the editorial staff))
Revised: ((will be filled in by the editorial staff))
Published online: ((will be filled in by the editorial staff))

[1] A. Kojima, K. Teshima, Y. Shirai, T. Miyasaka, J. Am. Chem. Soc. **2009**, 131, 6050.

[2] H.-S. Kim, C.-R. Lee, J.-H. Im, K.-B. Lee, T. Moehl, A. Marchioro, S.-J. Moon, R. Humphry-Baker, J.-H. Yum, J. E. Moser, M. Gratzel, N.-G. Park, Sci. Rep. **2012**, 2, 591.

[3] N. G. Park, J. Am. Chem. Soc. **2013**, 4, 2423.

[4] W. S. Yang, J. H. Noh, N. J. Jeon, Y. C. Kim, S. Ryu, J. Seo, S. I. Seok, Science **2015**, 348, 1234.

[5] M. M. Lee, J. Teuscher, T. Miyasaka, T. N. Murakami, H. J. Snaith, Science **2012**, 338, 643.

[6] M. Liu, M. B. Johnston, H. J. Snaith, Nature **2013**, 501, 395.

[7] H. Zhou, Q. Chen, G. Li, S. Luo, T.-b. Song, H.-S. Duan, Z. Hong, J. You, Y. Liu, Y. Yang, Science **2014**, 345, 542.

[8] D. Bi, W. Tress, M. I. Dar, P. Gao, J. Luo, C. Renevier, K. Schenk, A. Abate, F. Giordano, J.-P. C. Baena, J.-D. Decoppet, S. M. Zakeeruddin, M. K. Nazeeruddin, M. Grätzel, A. Hagfeldt, Sci. Adv. **2016**, 2, e1501170.

[9] W. Chen, Y. Wu, Y. Yue, J. Liu, W. Zhang, X. Yang, H. Chen, E. Bi, I. Ashraful, M. Grätzel, L. Han, Science **2015**, 350, 944.

[10] D. P. McMeekin, G. Sadoughi, W. Rehman, G. E. Eperon, M. Saliba, M. T. Hörantner, A. Haghighirad, N. Sakai, L. Korte, B. Rech, M. B. Johnston, L. M. Herz, H. J. Snaith, Science **2016**, 351, 151.

[11] Q. Wang, Q. Dong, T. Li, A. Gruverman, J. Huang, Adv. Mater. **2016**, DOI: 10.1002/adma.201600969.

[12] C. C. Stoumpos, M. G. Kanatzidis, Adv. Mater. **2016**, DOI: 10.1002/adma.201600265.

[13] D. Bi, P. Gao, R. Scopelliti, E. Oveisi, J. Luo, M. Grätzel, A. Hagfeldt, M. K. Nazeeruddin, Adv. Mater. **2016**, 28, 2910.

[14] M. Yang, Y. Zhou, Y. Zeng, C.-S. Jiang, N. P. Padture, K. Zhu, Adv. Mater. **2015**, 27, 6363.

[15] J. H. Heo, D. H. Song, H. J. Han, S. Y. Kim, J. H. Kim, D. Kim, H. W. Shin, T. K. Ahn, C. Wolf, T.-W. Lee, S. H. Im, Adv. Mater. **2015**, 27, 3424.

[16] T. Liu, K. Chen, Q. Hu, R. Zhu, Q. Gong, Adv. Energy Mater. **2016**, DOI: 10.1002/aenm.201600457.

[17] Z. Zhu, Y. Bai, X. Liu, C.-C. Chueh, S. Yang, A. K. Y. Jen, Adv. Mater. **2016**, DOI: 10.1002/adma.201600619.

[18] A. R. Pascoe, S. Meyer, W. Huang, W. Li, I. Benesperi, N. W. Duffy, L. Spiccia, U. Bach, Y.-B. Cheng, Adv. Funct. Mater. **2016**, 26, 1278.

[19] W.-Q. Wu, F. Huang, D. Chen, Y.-B. Cheng, R. A. Caruso, Adv. Energy Mater. **2016**, 6, DOI: 10.1002/aenm.201502027.

[20] W.-J. Yin, T. Shi, Y. Yan, Adv. Mater. **2014**, 26, 4653.

[21] W.-J. Yin, T. Shi, Y. Yan, Appl. Phys. Lett. **2014**, 104, 063903

[22] W.-J. Yin, T. Shi, Y. Yan, J. Phys. Chem. C **2015**, 119, 5253.

[23] W.-J. Yin, J.-H. Yang, J. Kang, Y. Yan, S.-H. Wei, J. Mater. Chem. A **2015**, 3, 8926.

[24] C. C. Stoumpos, L. Frazer, D. J. Clark, Y. S. Kim, S. H. Rhim, A. J. Freeman, J. B. Ketterson, J. I. Jang, M. G. Kanatzidis, J. Am. Chem. Soc. **2015**, 137, 6804.

[25] F. Hao, C. C. Stoumpos, D. H. Cao, R. P. H. Chang, M. G. Kanatzidis, Nat. Photon. **2014**, 8, 489.

[26] N. K. Noel, S. D. Stranks, A. Abate, C. Wehrenfennig, S. Guarnera, A. Haghighirad, A. Sadhanala, G. E. Eperon, S. K. Pathak, M. B. Johnston, A. Petrozza, L. Herz, H. Snaith, Energy Environ. Sci. **2014**, 7, 3061.

[27] B. Saparov, F. Hong, J.-P. Sun, H.-S. Duan, W. Meng, S. Cameron, I. G. Hill, Y. Yan, D. B. Mitzi, Chem. Mater. **2015**, 27, 5622.

[28] B.-W. Park, B. Philippe, X. Zhang, H. Rensmo, G. Boschloo, E. M. J. Johansson, Adv. Mater. **2015**, 27, 6806.

[29] F. Hong, B. Saparov, W. Meng, Z. Xiao, D. B. Mitzi, Y. Yan, J. Phys. Chem. C **2016**, 120, 6435.

[30] B. Saparov, D. B. Mitzi, Chem. Rev. **2016**, 116, 4558.

[31] M. H. Kumar, S. Dharani, W. L. Leong, P. P. Boix, R. R. Prabhakar, T. Baikie, C. Shi, H. Ding, R. Ramesh, M. Asta, M. Graetzel, S. G. Mhaisalkar, N. Mathews, Adv. Mater. **2014**, 26, 7122.

[32] F. Hao, C. C. Stoumpos, P. Guo, N. Zhou, T. J. Marks, R. P. H. Chang, M. G. Kanatzidis, J. Am. Chem. Soc. **2015**, 137, 11445.

[33] S. J. Lee, S. S. Shin, Y. C. Kim, D. Kim, T. K. Ahn, J. H. Noh, J. Seo, S. I. Seok, J. Am. Chem. Soc. **2016**, 138, 3974.

[34] M.-C. Jung, S. R. Raga, Y. Qi, RSC Adv. **2016**, 6, 2819.

[35] M. Zhang, M. Lyu, J.-H. Yun, M. Noori, X. Zhou, N. A. Cooling, Q. Wang, H. Yu, P. C. Dastoor, L. Wang, Nano Research **2016**, 1.

[36] T. Yokoyama, D. H. Cao, C. C. Stoumpos, T.-B. Song, Y. Sato, S. Aramaki, M. G. Kanatzidis, J. Phys. Chem. Lett. **2016**, 7, 776.

[37] T. M. Koh, T. Krishnamoorthy, N. Yantara, C. Shi, W. L. Leong, P. P. Boix, A. C. Grimsdale, S. G. Mhaisalkar, N. Mathews, J. Mater. Chem. A **2015**, 3, 14996.

[38] I. Chung, B. Lee, J. He, R. P. H. Chang, M. G. Kanatzidis, Nature **2012**, 485, 486.

[39] N. J. Jeon, J. H. Noh, Y. C. Kim, W. S. Yang, S. Ryu, S. I. Seok, Nat. Mater. **2014**, 13, 897.

[40] W. Ke, C. Xiao, C. Wang, B. Saparov, H.-S. Duan, D. Zhao, Z. Xiao, P. Schulz, S. P. Harvey, W. Liao, W. Meng, Y. Yu, A. J. Cimaroli, C.-S. Jiang, K. Zhu, M. Al-Jassim, G. Fang, D. B. Mitzi, Y. Yan, Adv. Mater. **2016**, 28, 5214.

[41] N. Ahn, D.-Y. Son, I.-H. Jang, S. M. Kang, M. Choi, N.-G. Park, J. Am. Chem. Soc. **2015**, 137, 8696.

[42] P. Peumans, S. R. Forrest, Appl. Phys. Lett. **2001**, 79, 126.

[43] D. Zhao, M. Sexton, H.-Y. Park, G. Baure, J. C. Nino, F. So, Adv. Energy Mater. **2015**, 5, 1401855.

[44] Z. Xiao, C. Bi, Y. Shao, Q. Dong, Q. Wang, Y. Yuan, C. Wang, Y. Gao, J. Huang, Energy Environ. Sci. **2014**, 7, 2619.

[45] D. Zhao, W. Ke, C. R. Grice, A. J. Cimaroli, X. Tan, M. Yang, R. W. Collins, H. Zhang, K. Zhu, Y. Yan, Nano Energy **2016**, 19, 88.

[46] W. Ke, D. Zhao, C. R. Grice, A. J. Cimaroli, G. Fang, Y. Yan, J. Mater. Chem. A **2015**, 3, 23888.

[47] S. Sun, T. Salim, N. Mathews, M. Duchamp, C. Boothroyd, G. Xing, T. C. Sum, Y. M. Lam, Energy Environ. Sci. **2014**, 7, 399.

[48] D. W. Zhao, X. W. Sun, C. Y. Jiang, A. K. K. Kyaw, G. Q. Lo, D. L. Kwong, Appl. Phys. Lett. **2008**, 93, 083305.

[49] J.-Y. Jeng, Y.-F. Chiang, M.-H. Lee, S.-R. Peng, T.-F. Guo, P. Chen, T.-C. Wen, Adv. Mater. **2013**, 25, 3727.

[50] F. Wang, J. Ma, F. Xie, L. Li, J. Chen, J. Fan, N. Zhao, Adv. Funct. Mater. **2016**, 26, 3417.

[51] Y. Ogomi, A. Morita, S. Tsukamoto, T. Saitho, N. Fujikawa, Q. Shen, T. Toyoda, K. Yoshino, S. S. Pandey, T. Ma, S. Hayase, J. Phys. Chem. Lett. **2014**, 5, 1004.

[52] F. Hao, C. C. Stoumpos, R. P. H. Chang, M. G. Kanatzidis, J. Am. Chem. Soc. **2014**, 136, 8094.

[53] Y. Shao, Z. Xiao, C. Bi, Y. Yuan, J. Huang, Nat. Commun. **2014**, 5.

[54] D. Bi, L. Yang, G. Boschloo, A. Hagfeldt, E. M. J. Johansson, J. Phys. Chem. Lett. **2013**, 4, 1532.

[55] L. J. A. Koster, V. D. Mihailetchi, H. Xie, P. W. M. Blom, Appl. Phys. Lett. **2005**, 87, 203502.

[56] V. D. Mihailetchi, J. Wildeman, P. W. M. Blom, Phys. Rev. Lett. **2005**, 94, 126602.

[57] A. K. K. Kyaw, D. H. Wang, V. Gupta, W. L. Leong, L. Ke, G. C. Bazan, A. J. Heeger, ACS Nano **2013**, 7, 4569.

[58] S. R. Cowan, A. Roy, A. J. Heeger, Phys. Rev. B **2010**, 82, 245207.

[59] M. M. Mandoc, F. B. Kooistra, J. C. Hummelen, B. de Boer, P. W. M. Blom, Appl. Phys. Lett. **2007**, 91, 263505.

[60] S. R. Cowan, W. L. Leong, N. Banerji, G. Dennler, A. J. Heeger, Adv. Funct. Mater. **2011**, 21, 3083.

[61] R. N. Hall, Phys. Rev. **1952**, 87, 387.

[62] W. Shockley, W. T. Read, Phys. Rev. **1952**, 87, 835.

[63] Y. Dang, Y. Zhou, X. Liu, D. Ju, S. Xia, H. Xia, X. Tao, Angew. Chem. Int. Ed. **2016**, 55, 3447.

[64] C. C. Stoumpos, C. D. Malliakas, M. G. Kanatzidis, Inorg. Chem. **2013**, 52, 9019.

[65] I. J. Bruno, J. C. Cole, P. R. Edgington, M. Kessler, C. F. Macrae, P. McCabe, J. Pearson, R. Taylor, Acta Crystallographica Section B **2002**, 58, 389.

[66] D. K. Schroder, *Semiconductor material and device characterization*, Wiley, 1990.

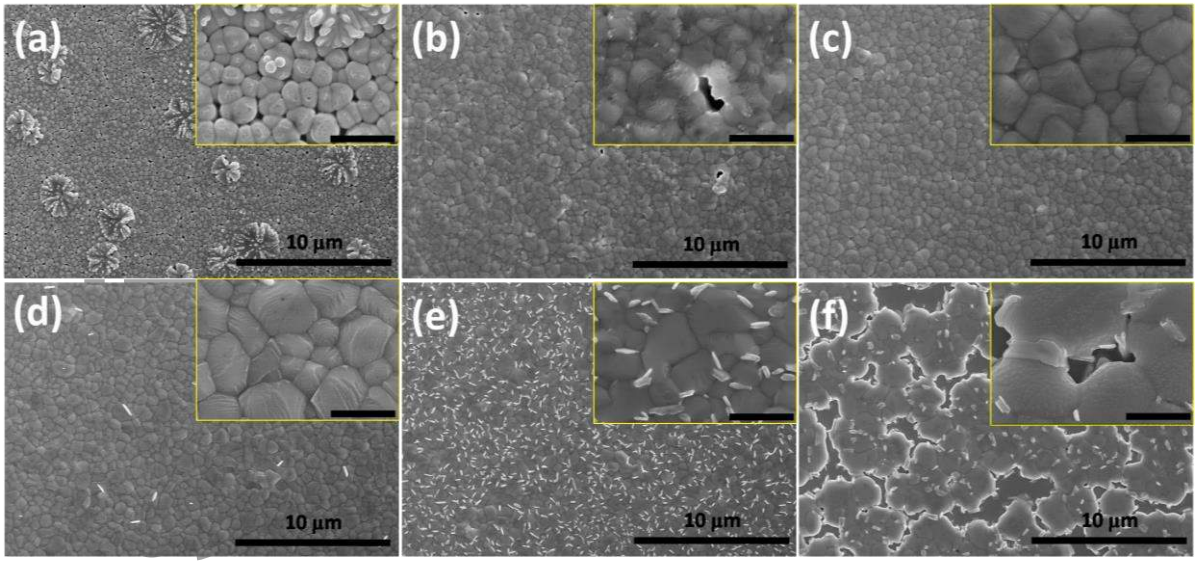

Figure 1. SEM images of $FASnI_3$ perovskite films on PEDOT:PSS with varying concentration of SnF_2: (a) 0 mol%, (b) 5 mol%, (c) 10 mol%, (d) 15 mol%, (e) 20 mol%, (f) 30 mol%. Scale bar in all images is 10µm. The inset in each figure shows their corresponding SEM image with high magnification. The scale bar in the inset is 1 µm.

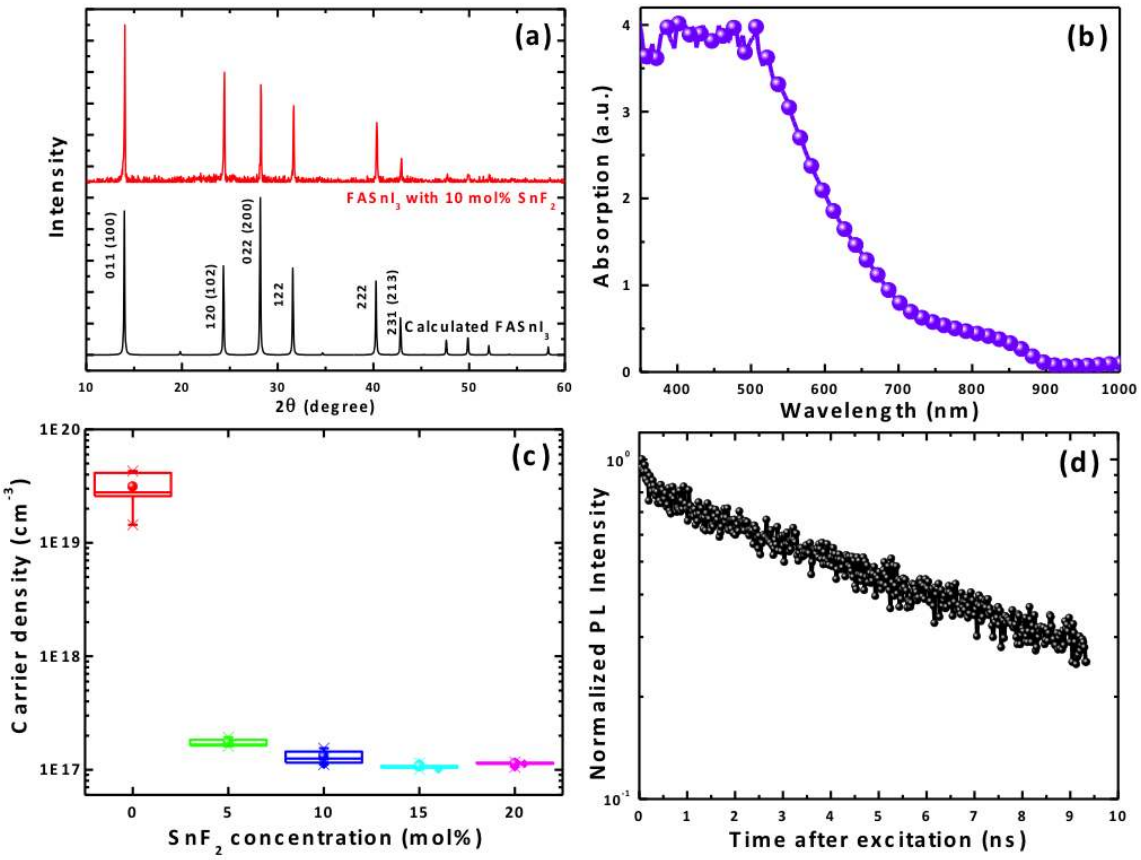

Figure 2. (a) XRD patterns of $FASnI_3$ perovskite film with 10 mol% SnF_2 and calculated orthorhombic structure of $FASnI_3$. (b) Absorption spectrum of $FASnI_3$ film with 10 mol% SnF_2 on PEDOT:PSS. (c) Carrier density versus SnF_2 molar concentration in $FASnI_3$ PVSCs. (d) TRPL decay of a $FASnI_3$ film with 10 mol% SnF_2.

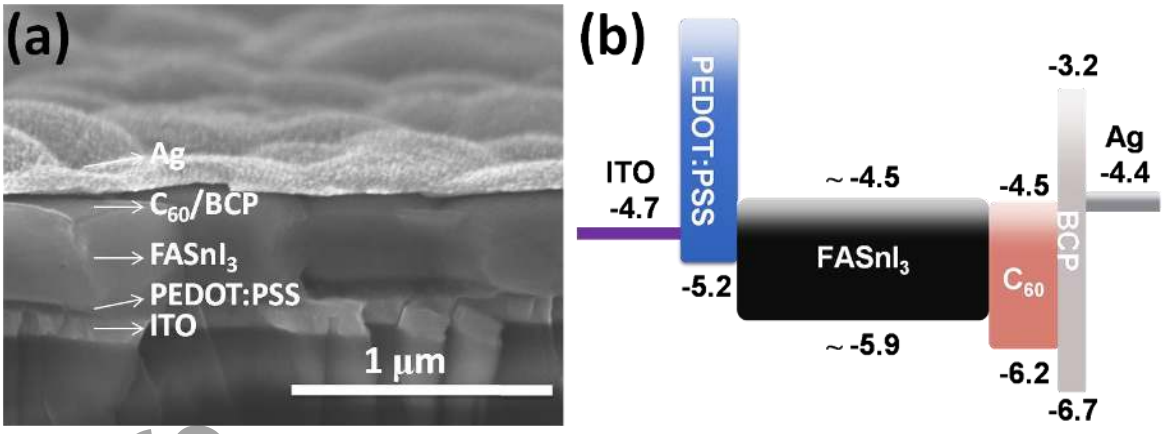

Figure 3. (a) Cross-sectional SEM image of our entire device with 10 mol% SnF_2 additives, in which each layer is labeled. (b) Schematic of energy level diagram of our $FASnI_3$ perovskite solar cells.

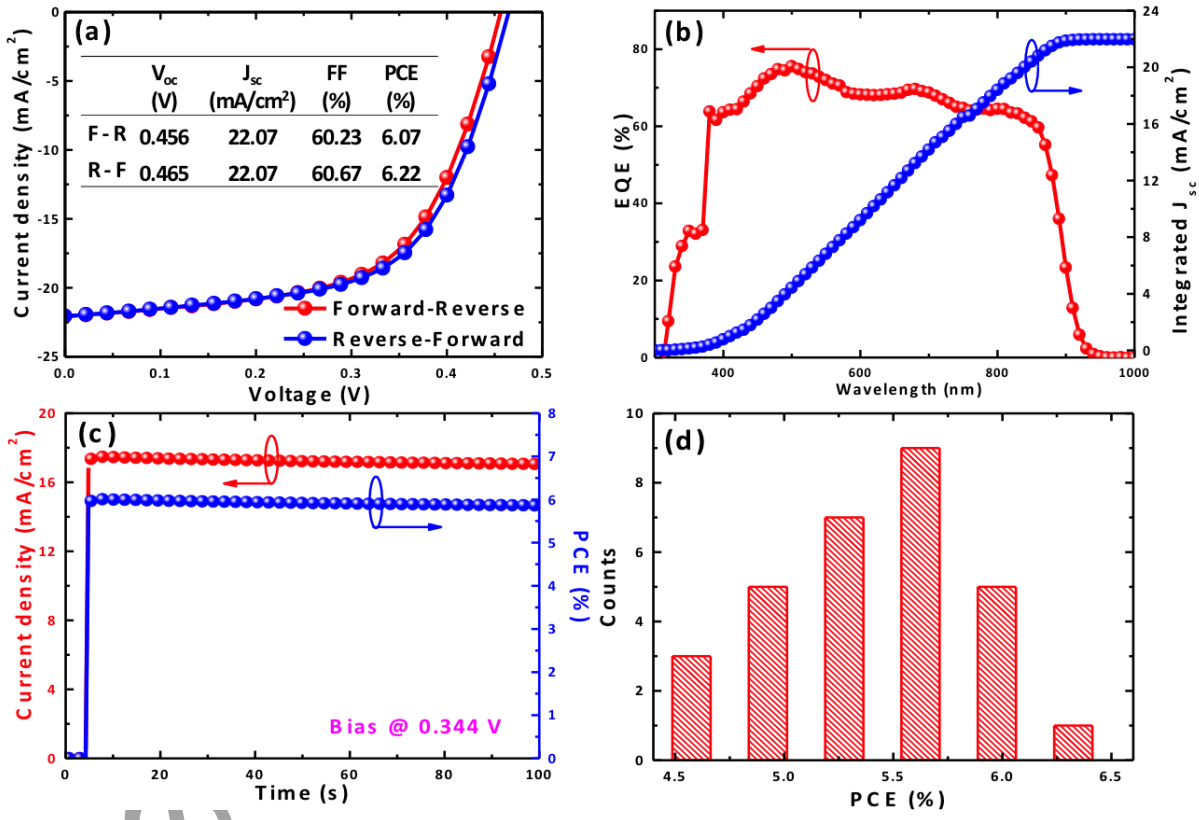

Figure 4. (a) *J-V* characteristics under 100 mW/cm^2 AM1.5G illumination under reverse and forward voltage scans, (b) EQE spectrum and integrated J_{sc}, (c) Steady-state J_{sc} and PCE at a constant bias of 0.344 V under 100 mW/cm^2 illumination, of our champion cell with 10% SnF_2 additives, (d) PCE histogram of 30 devices with 10% SnF_2 additives from several fabrication batches of solar cells.

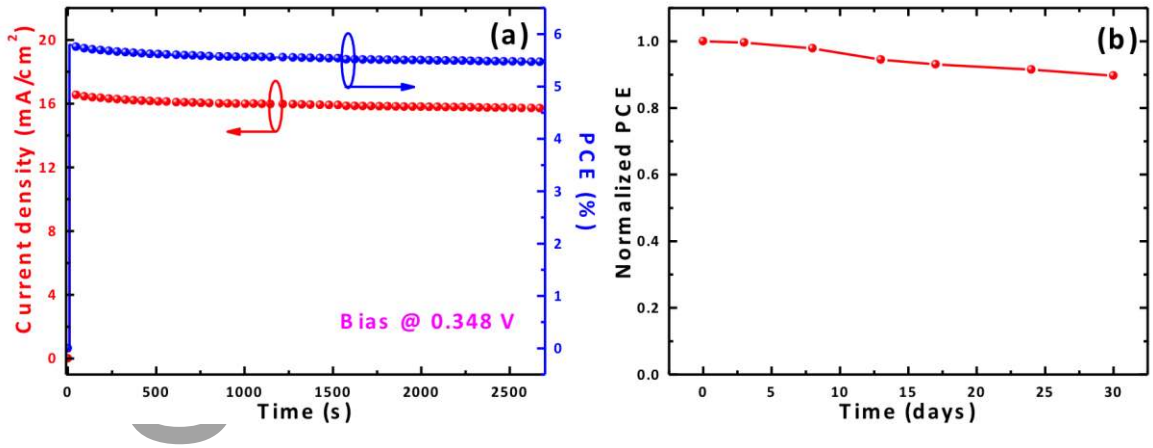

Figure 5. (a) Steady-state efficiency and photocurrent density versus time under continuous 100 mW/cm^2 AM1.5G illumination at a constant bias of 0.348 V. (b) Stability of our encapsulated cell with 10 mol% SnF_2 additives measured in ambient.

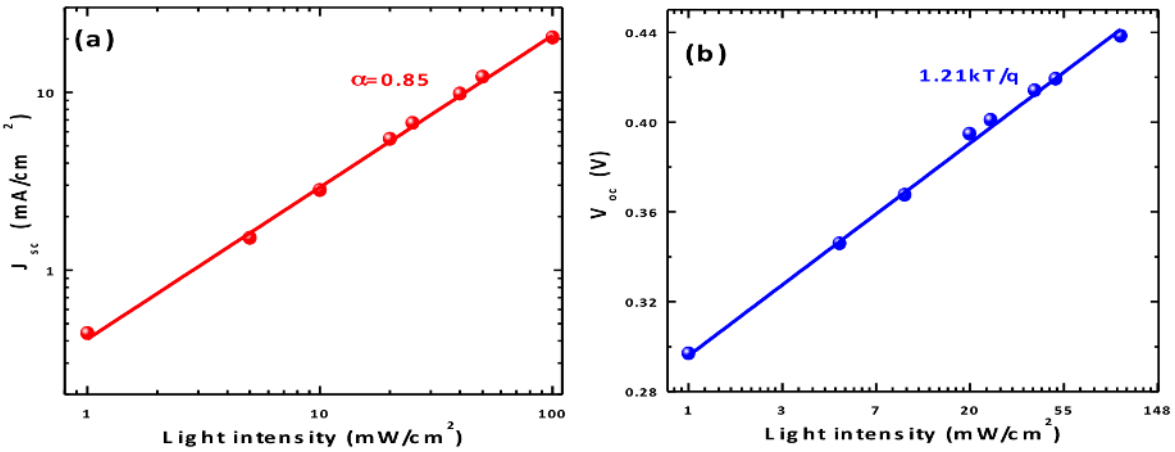

Figure 6. Light-intensity dependence of $FASnI_3$ PVSC performance with 10 mol% SnF_2 additives: (a) J_{sc} versus light intensity and (b) V_{oc} versus light intensity. The light intensity ranges from 1 to 100 mW/cm^2

The table of contents:

Efficient lead (Pb)-free inverted planar formamidinium tin triiodide ($FASnI_3$) perovskite solar cells (PVSCs) have been demonstrated. Along with solvent engineering, diethyl ether dripping leads to highly uniform and pinhole-free compact $FASnI_3$ films withsuitable carrier density for solar cell application. Our $FASnI_3$ PVSCs with 10 mol% SnF_2 additives have achieved average power conversion efficiencies (PCEs) of 5.41±0.46% and maximum PCE of 6.22% under forward voltage scan, exhibiting small*J-V*hysteresis and high reproducibility. The champion cell shows a steady-state efficiency of ~6.00% for over 100s. Theencapsulated cells have shown a good long-term illumination stability with a 5.50% decrease of its initial efficiency of 5.80% over a period of 2700 s.

Keyword: Pb-free perovskite solar cells, $FASnI_3$, pinhole-free, uniform perovskite, SnF_2 additives

Lead-Free Inverted Planar Formamidinium Tin Triiodide Perovskite Solar Cells Achieving Power Conversion Efficiencies up to 6.22%

Weiqiang Liao,[†] Dewei Zhao, [†], Yue Yu, Corey R. Grice, Changlei Wang, Alexander J. Cimaroli, Philip Schulz, Weiwei Meng, Kai Zhu, Ren-Gen Xiong,* and Yanfa Yan**